Applied Surface Science Advances 1 (2020) 100024

Contents lists available at ScienceDirect

Applied Surface Science Advances

journal homepage: www.elsevier.com/locate/apsadv

Room temperature operated HgCdTe colloidal quantum dot infrared focal plane array using shockwave dispersion technique

Abhijit Chatterjee[a,*], Janani Balakrishnan[b], Naresh Babu Pendyala[a], K.S.R. Koteswara Rao[b]

[a] Space Applications Centre (ISRO), Sensors Development Area, Ahmedabad 380015, India
[b] Department of Physics, Indian Institute of Science, Bangalore 560012, India

ARTICLE INFO

Keywords:
CQD
FPA
MWIR
D*
ROIC

ABSTRACT

This paper reports development and performance evaluation of room temperature operated Mercury Cadmium Telluride (HgCdTe) colloidal quantum dot (CQD) coated Si Readout Integrated Circuit (ROIC) based Infrared (IR) Focal Plane Array (FPA). HgCdTe CQD has been synthesized through bottom up chemical approach and coated over commercially off-the-shelf (COTS) Si ROIC die using indigenously developed Shock Wave Dispersion Technique to achieve better uniformity, thickness control and adhesion to Si ROIC compared to spin coating or drop casting, better absorption of photons which resulted in improved imaging performance. Images of various IR and visible targets have been captured and performance analysis has been carried out and detectivity of 4.8×10^7 Jones achieved at room temperature for IRFPA fabricated by new material deposition technique. Temperature dependent photo-response variation of the IR FPA also has been evaluated to determine optimum operating temperature.

1. Introduction

The dominant photon detectors and FPAs in the mid-wave infrared (MWIR) spectral range use single crystal InSb and HgCdTe materials [1–3], however, low-temperature cooling is required, which increases the occupied space and energy consumption of the detector, requiring bulky imaging instrument. Motivation of this research work is to synthesize HgCdTe quantum dots responsive in MWIR spectral range using chemical synthesis method and develop low cost room temperature operated IR FPA using combination of commercial silicon ROIC and synthesized HgCdTe CQD layer. For quantum dots of a composition, the minimum possible band gap is controlled by the composition, and the maximum band gap is based on the size of the particle, which can be tuned using low cost [4] chemical synthesis method. $Hg_{1-x}Cd_xTe$ is a potential candidate owing to its features, such as a negative band gap $E_G = -0.15$ eV and large excitonic Bohr radius, ensuring the quantum confinement effect at the desired spectral range where x is the Cd mole fraction. Solid state grown detector array technology involves MBE growth, process steps like lithography, etching, metal deposition and finally the flip-chip bonding. All these steps and yield issues make the solid state IRFPAs costlier. Whereas, in the present device fabrication, directly coating of solution is carried out on ROIC and so cost effective. We have followed similar chemical synthesis method for HgCdTe CQD and selection of COTS ROIC from our previous work [5] where spin coating technique was adopted to develop photosensitive layer over ROIC. Deposition of quantum-structures on the substrates of choice towards formation of either contacts (Ohmic or Schottky) or heterostructures and superlattices is one of the major challenges in the effective utility of nanostructures in the device applications [6–8]. A first study has been done in this direction by coupling HgTe and HgSe materials in hetero-structured nanocrystals [9,10]. These core-shell structures help to improve photo response by CQD films. Development of HgTe based IRFPA has been reported [11–14] where tuning the capping ligands is carried out to adjust the material from the p-type to ambipolar. Research on plasmonic structures mentioned in [15–17] and resonant cavity-based structures [18,19] are also promising candidates for IR detection. Response time of CQD based photodetectors in MWIR range is also quite fast and better than bolometers at room temperature [20]. Major evaporation and growth techniques currently in practice for QDs deposition are Molecular Beam Epitaxy (MBE), Chemical Vapor Deposition (CVD), Sputtering, Langmuir-Blodgett technique, Spin-coating, and Drop-casting. Among them the MBE/ CVD techniques being highly sophisticated, which combines both growth and dispersion, addresses this issue effectively [21]. The spin-coating method is not only limited to planar substrates but also the problem of inter-diffusion between the layers during the formation of heterostructures as well as wastage of base material is very high. Research has been carried out for deposition of atomized QDs solution by a pressurized N_2 nozzle for visible and NIR range [22]. Air-processed patterning method has been adopted to produce flexible room temperature multicolor MWIR detector [23] with responsivity 0.9A/W. In the present technique (RARE SD-NBE) [24], low intensity shockwaves have been generated to disperse QDs on Si

* Corresponding author.
E-mail address: abhijit@sac.isro.gov.in (A. Chatterjee).

https://doi.org/10.1016/j.apsadv.2020.100024
Received 29 May 2020; Received in revised form 18 August 2020; Accepted 18 August 2020
Available online 26 August 2020

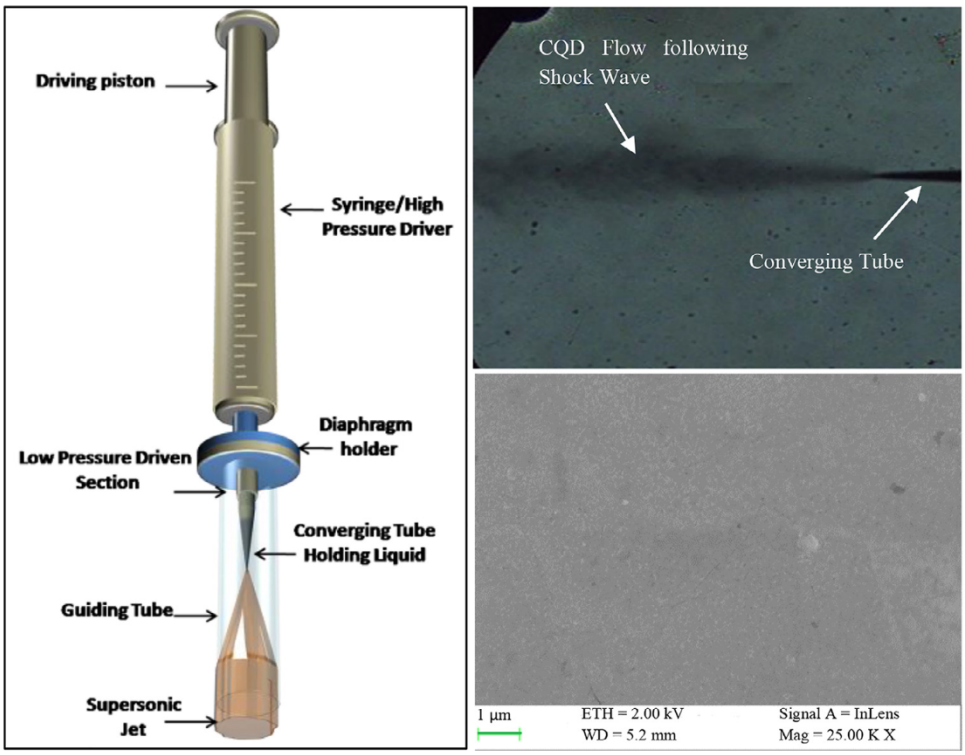

Fig. 1. (a) Schematic diagram of shock wave setup. (b) Flow of colloids containing QDs that follows the shock wave. (c) SEM images of CQD layer deposited by shockwave technique on Si substrate

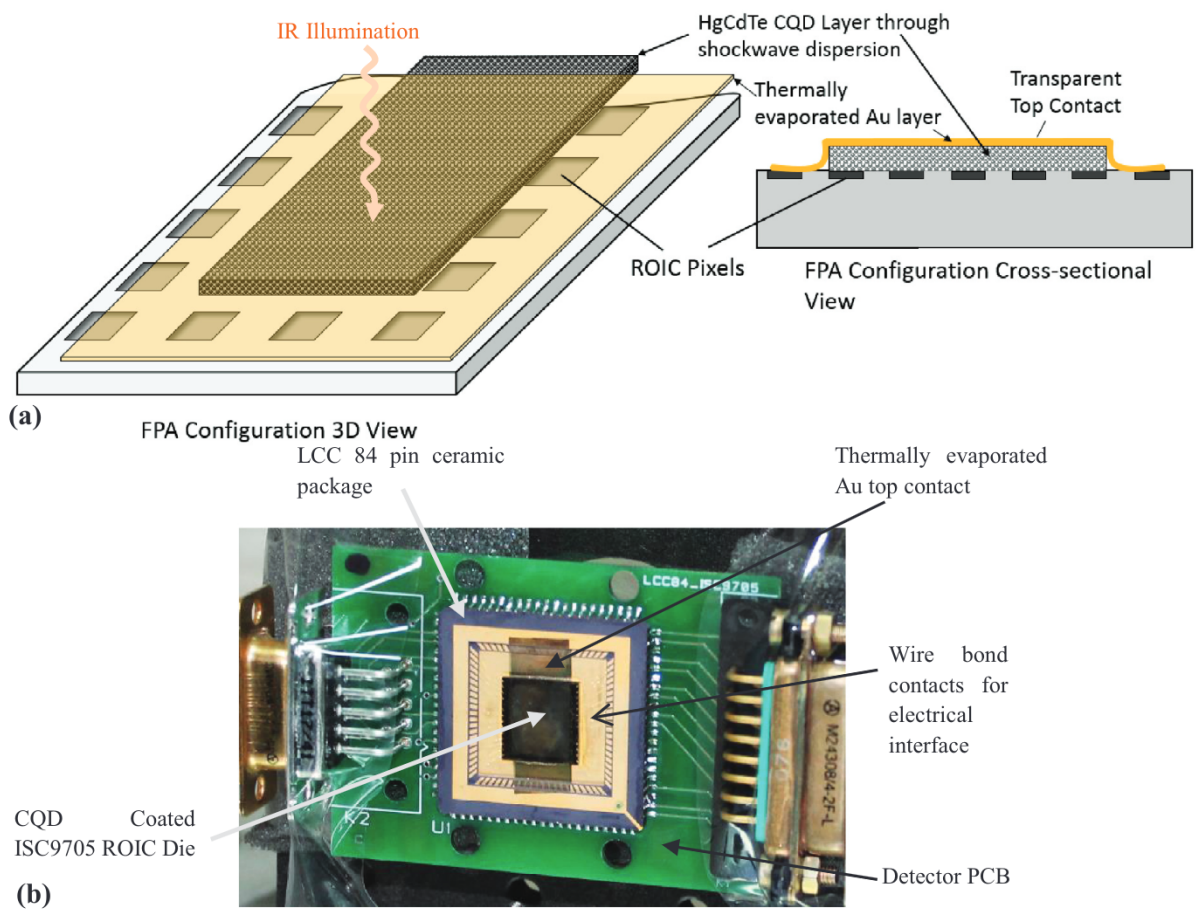

Fig. 2. (a) Modified FPA configuration. (b) Actual photograph of modified FPA after soldering on interface PCB.

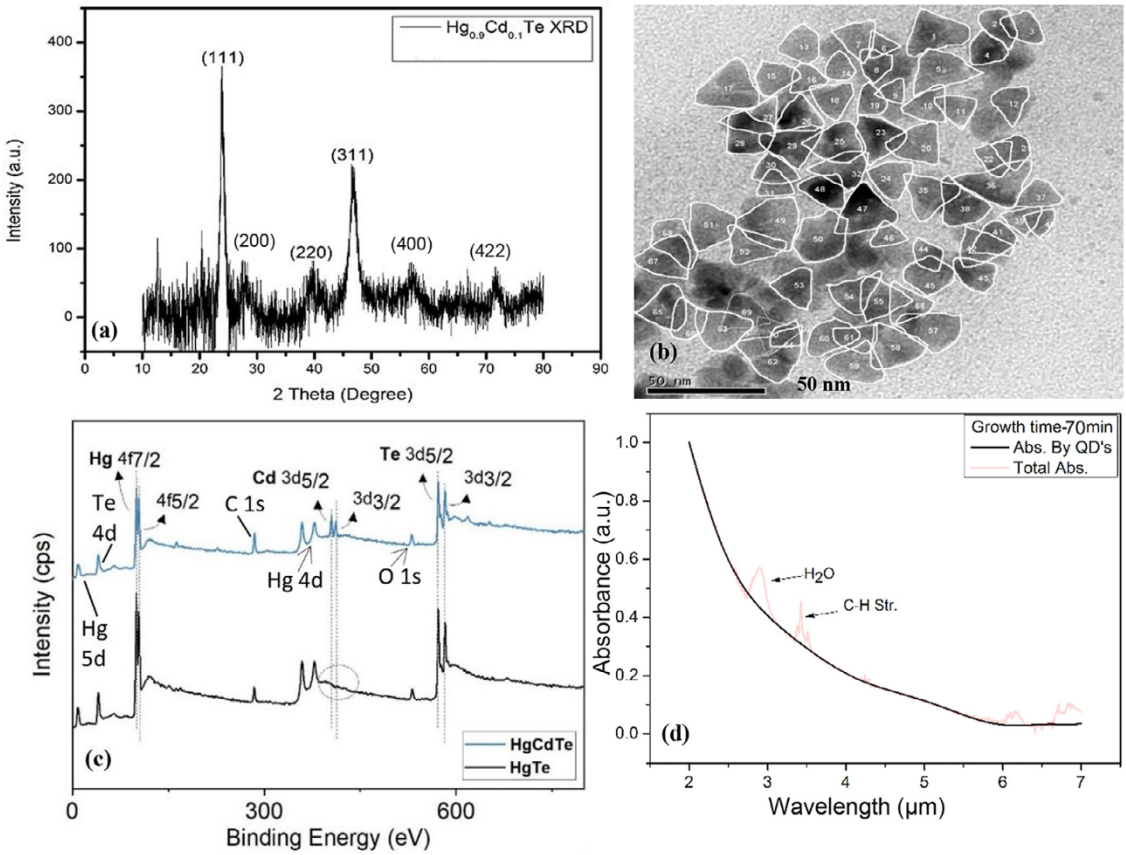

Fig. 3. (a) XRD plot of HgCdTe CQDs indicating growth facets. (b) TEM image of synthesized HgCdTe CQD (c) XPS plot of HgCdTe and HgTe CQD. (d) Absorption spectrum of CQD.

ROIC die. Essentially the aerodynamic processes include formation of a shock wave followed by supersonic flow sandwiched between the driver gas and the shock front. The strength of the shock wave is measured in terms of Mach number [25], which is greater than 1. Fig. 1(a) shows the shock tube which consists of a tube of constant area divided into high pressure driver and low pressure driven sections separated by a thin diaphragm. Sudden rupture of the diaphragm due to increase in the gas inside the driver section generates a shock wave travelling in to the low pressure driven section. When gas expands impulsively from confined high pressure area to low pressure area due to the rupture in diaphragm, the air molecules travel at speeds greater than the speed of the sound (supersonic and hypersonic) into the low pressure driven tube. Fig. 1(b) shows the flow of CQD due to shock wave captured by high frame rate camera. Scanning Electron Microscopy (SEM) image of the deposited CQD over Si substrate is shown in Fig. 1(c). Influence of the layer thickness in plasmonic gold nanoparticles produced by thermal evaporation for different gold layer thickness has been reported in [26] where significant transmittance is observed for SWIR and MWIR spectral ranges [27]. We have used thermally evaporated gold thin film (~ 7nm) as common transparent contact for ROIC pixels (VDETCOM) instead of graphene oxide used in older FPA configuration mentioned in our previous work [5]. Significant amount of imaging performance improvement has been observed with IRFPA developed by mentioned material deposition technique. Low temperature response variation has been carried out using temperature-controlled cryostat.

2. FPA development and experimental work

Modified FPA configuration has been shown in Fig. 2(a) where isometric and cross-sectional schematic are shown. HgCdTe CQD layer of

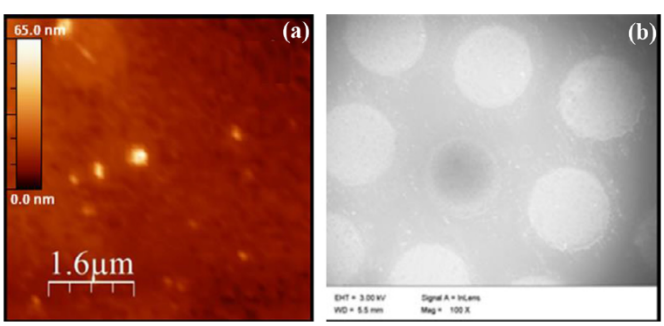

Fig. 4. (a) AFM image of the CQD film with measured average thickness of 50±5 nm. (b) SEM images of patterned CQDs on Si substrate.

thickness ~ 200nm is deposited through shockwave dispersion technique and the CQD coated 320 × 256 pixels ROIC die [28] is attached to LCC 84 pin ceramic package. Thermally evaporated gold thin film layer of thickness ~ 7 nm deposited as transparent top contact after wire bonding of the die to package. Realized FPA mounted in PCB is shown in Fig. 2(b). Uniformity of the CQD film has been verified by photo-response non-uniformity (PRNU) measurement of FPA using a uniform light source which resulted in PRNU ~ 1% for entire array excluding dead pixels. Photo-generated charge carriers are hopped [29] through the quantum dots which are in physical contact with ROIC pixel pad and contribute to photocurrent. Detailed experimental study of carrier dynamics resonantly pumped at the band edge in the MWIR and far above the band edge for HgTe QD where fast photo-response of > 50MHz has been achieved [30]. Direct Injection readout circuit of ROIC converts the photocurrent into voltage which is acquired through National

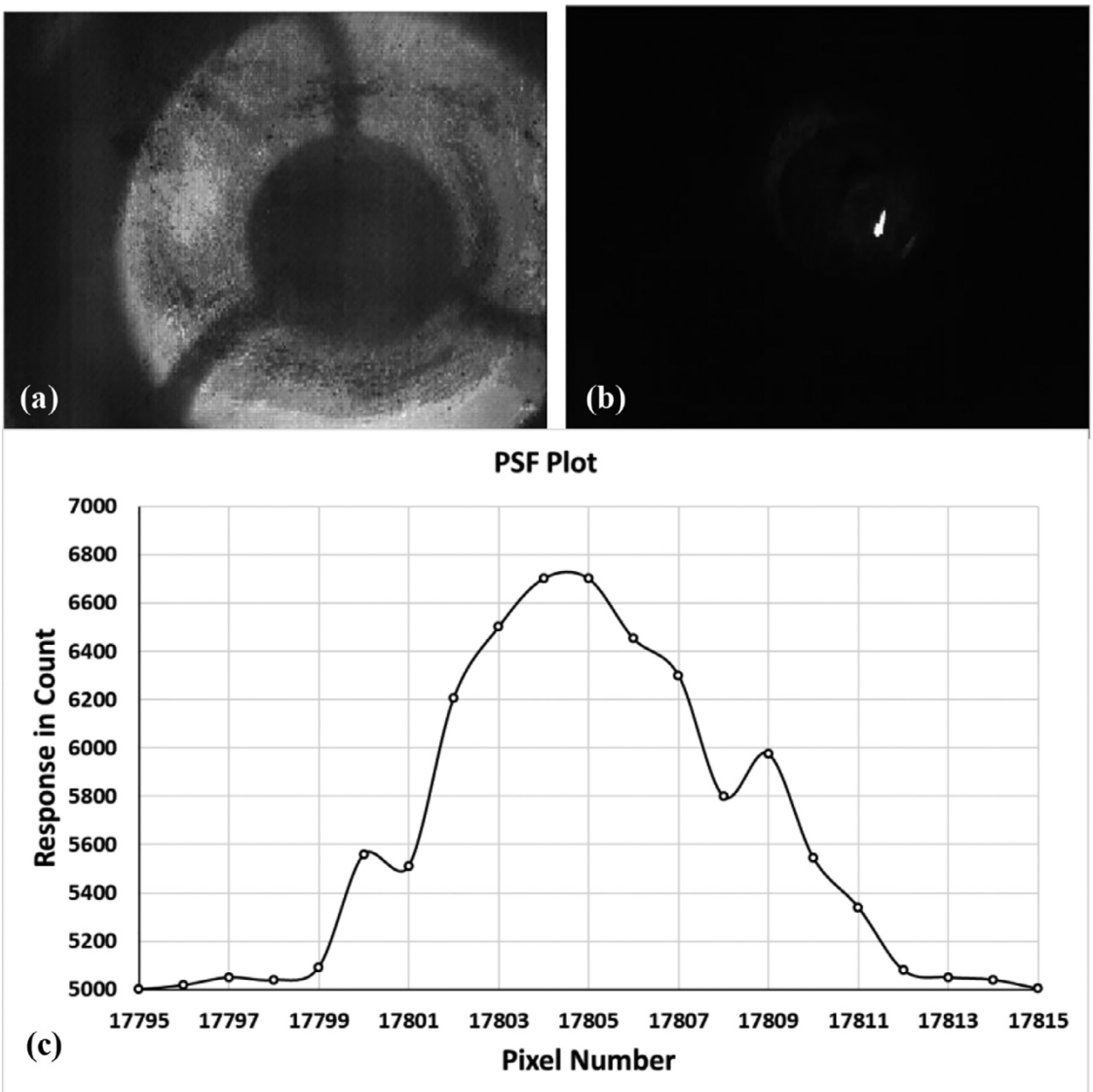

Fig. 5. (a) Image of IR lamp through RC microscopic objective in defocused condition where secondary mirror spiders are visible. (b) IR spot after focusing. (c) Pixel response shows dark offset is around 5000 digital count and illuminated region response is 6700 counts. Spread is around 10 pixels.

Instruments PXI data acquisition (DAQ) unit. A Zinc Selenide f/2.0 IR lens having transmission in 1μm-18μm spectral range has been used as focusing optics and different IR targets are being imaged. Room temperature imaging has been carried out for different targets. Same FPA has been operated at low temperature (120–280 K) by mounting it inside a temperature-controlled cryostat to evaluate temperature dependent photo-response and optimum operating condition.

3. Experimental test results

X-ray diffraction (XRD) plot (Fig. 3(a)) of synthesized CQD shows six peaks, which corresponds to the (111), (200), (220), (311), (400) and (422) planes of cubic zinc blende structure of CdTe and HgTe. TEM image (Fig. 3(b)) shows formation of tetrahedral HgCdTe nano crystals XPS elemental analysis of CQD is shown in Fig. 3(c). Similar results have been reported in our previous work on HgCdTe CQD [31]. Fig. 3(d) shows the absorption spectrum, confirms absorption up to MWIR range. Fig. 4(a) shows the AFM image of uniform CQD film (roughness ~ 60nm) deposited over Si substate and Fig. 4(b) shows the SEM image of patterned CQD over Si substrate.

Indigenously developed FPA shows significant response to IR radiation at room temperature and electro-optical parameters like MTF, Responsivity, Quantum Efficiency, Specific Detectivity (D*) have been computed.

Edmond optics make RC Microscopic Objective has been used as focusing optics for evaluation of impulse response through localized IR spot and Fig. 5 shows the point spread function (PSF) response of the FPA having spread of around ten pixels. Fast Fourier Transform (FFT) of the PSF has been computed to evaluate Modulation Transfer Function (MTF) of the FPA which is a combined MTF of sensor and optics. ROIC used for this FPA development has pixel dimension of 8μm × 8μm and pitch of 30μm.Hence, spatial Nyquist frequency is ~ 16 lp/mm. FFT plot of the PSF (Fig. 6) shows MTF value of around 10% at Nyquist compared to 5.5% of previous version FPA (shown in inset of Fig. 6). This is a significant improvement from previously developed FPA where adhesion of QD with FPA pixel, CQD layer uniformity, charge transfer and transparent top contact played an important role.

Hot soldering iron at 300°C has been imaged through this FPA inside dark room at room temperature. Image of hot solder iron taken by FPA has been shown in Fig. 7(a) and corresponding histogram of response counts is shown in Fig. 7(b). Histogram shows 3500 count variation

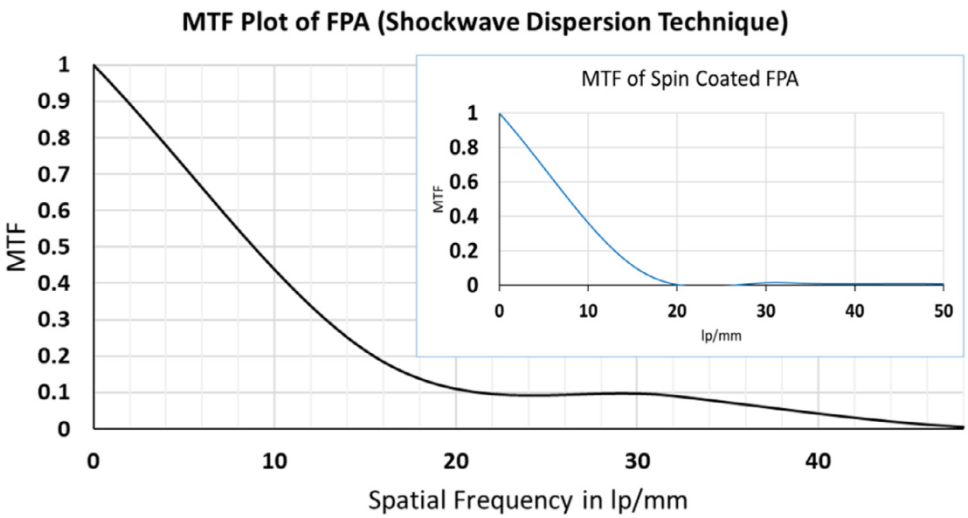

Fig. 6. MTF plot of FPA computed by performing FFT of PSF. MTF shown is the combined MTF of optics and FPA. MTF plot shown in the inset is of spin coated version of FPA.

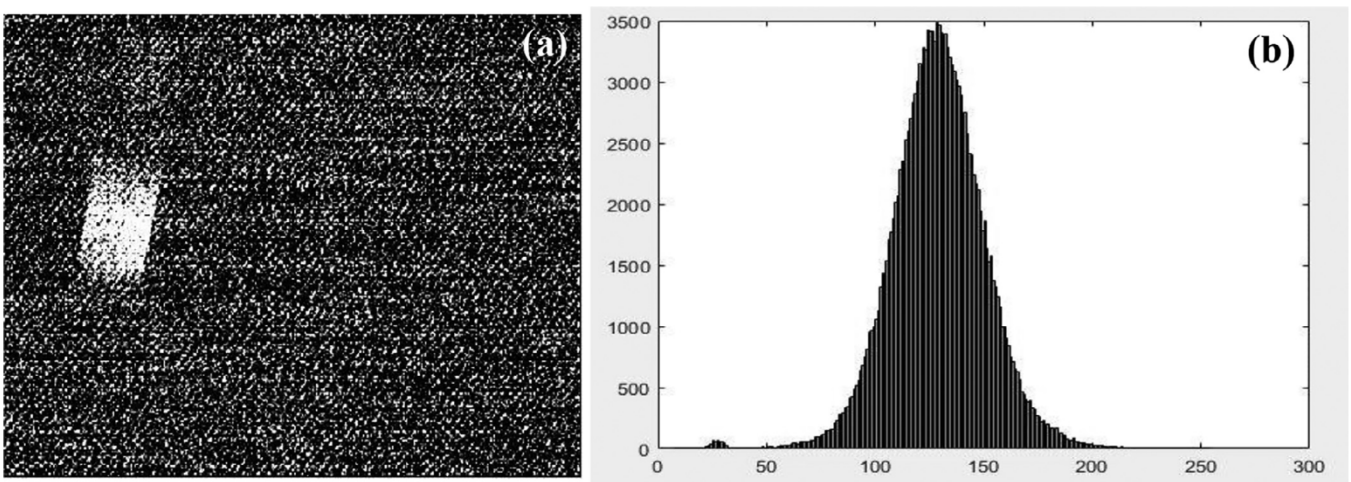

Fig. 7. (a) Image of hot soldering iron at room temperature inside dark room. (b) corresponding histogram plot of response vs number of pixels.

over entire pixel range for solder iron target at room temperature. This response confirms IR sensitivity of the FPA and further performance parameters are evaluated based on this data.

From the standpoint of radiometry, the optical system transfers the radiance from the target to the focal plane. We shall now present the relationship between the target radiance and the instrument parameters. Consider an optical system with diameter D transferring radiance from the target to the detector at the focal plane. The radiant flux (power) delivered to the detector is given by

$$\phi_d = \frac{\pi}{4} O_e \Delta\lambda L_\lambda \beta^2 D^2 \text{ watts} \quad (1)$$

where L_λ is the target radiance ($W \cdot m^{-2} \cdot sr^{-1} \cdot \mu m^{-1}$) $\Delta\lambda$ is the spectral bandwidth of the radiation to be measured (μm) O_e is the optical efficiency—transmittance of the optical system including atmosphere (<1) β is the system geometric FOV; in remote sensing, usually referred to as instantaneous FOV (radians). If A_d is the detector area, $\beta^2 = A_d/f^2$, where f is the focal length; the aforementioned equation can be rewritten as follows:

$$\emptyset_d = \frac{\pi}{4} O_e \Delta\lambda L_\lambda \frac{A_d}{f^2} D^2 \text{ watts} \quad (2)$$

FPA Pixel Area $A_d = 64 \times 10^{-12}$ m^2, effective focal length of the optics f = 24 mm and clear aperture diameter D = 12 mm for f/2.0. Spectral radiance calculated for 300 °C target using Planck's law $\lambda L_\lambda = 115.5$ $W/m^2/Sr$ which result in $\emptyset_d = 1.15$ nW. Energy received by the FPA for integration time $\tau = 12.8$ mS is $\emptyset_d \times \tau = 14.7 \times 10^{-12}$ J.

If Þ is the number of photons,

$$\emptyset_d \times \tau = p \times \frac{hc}{\lambda} \quad (3)$$

Þ ≈ 2.22×10^8 for $\lambda = 3$ μm.

Maximum output analog swing of the FPA is 3 volt and it is digitized by a 14bit ADC in DAQ system. Conversion efficiency of the sensor is ~ 0.17 μV/e-.

Hence 1 least count = $\frac{3.0}{2^{14}}$ V ≈ 183μV. Count difference due to hot target = 3500 and corresponding output = 640.5mV which is equivalent to 3766000 photogenerated electrons (n_e). Hence, quantum efficiency

$$\eta = \frac{n_e}{p} \times 100 \approx 1.7\%$$

Readout noise of the FPA by computing standard deviation over 64 dark frame = 0.5 count ≈ 538e-. D^* of the FPA comes out to be 4.8×10^7 Jones for responsivity 41 mA/W. This comparable to the expected performance of the HgCdTe quantum dot detectors mentioned in [32].

Low temperature performance of this modified FPA has been evaluated using temperature-controlled cryostat. Dark reference has been recorded for each temperature and it is subtracted from illuminated value. Focused beam of IR lamp through ZnSe lens is used as IR source which is kept outside cryostat. Table 1. shows FPA response counts at different temperature and Fig. 8 shows temperature dependent response plot. The plot shows peak response at ~ 140K.

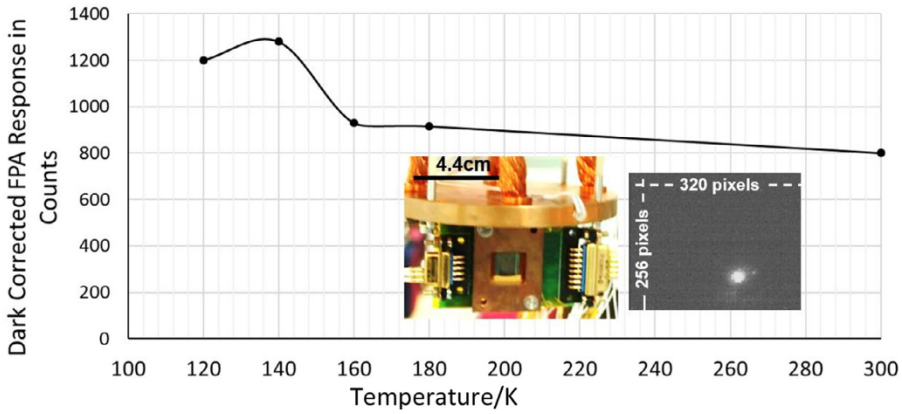

Fig. 8. Low temperature response of CQD FPA (Dark subtracted output) and image taken by FPA inside cryostat of IR source is kept in the inset and FPA photograph connected to cryostat cold finger.

Table 1
FPA response at different operating temperature.

Temperature/K	Dark Count	Illuminated Count	Dark Corrected Response
120	4800	6000	1200
140	4820	6100	1280
160	4860	5790	930
180	4900	5815	915
300	5010	5810	800

4. Conclusion

In conclusion, HgCdTe colloidal quantum dot based infrared focal plane array has been developed using shockwave dispersion technique and imaging at room temperature has been carried out using indigenously developed FPGA based test setup. Low temperature response of modified FPA has been carried out. Further improvement in the FPA response by changing chemical composition of CQD and electro-optical characterization will be carried out as future activities. Beyond the cost reduction, CQDs also present significant advantages such as reduced Auger effect that should help in the quest of increasing the operating temperature of IR sensors. Transport in NC arrays is usually done with a single NC population with a fine control of the size dispersity to avoid the largest particles to behave as trap states for the hopping carriers. Looking to the future of optoelectronic devices containing colloidal QDs, it seems that one of the major hurdles standing in their way is that many of the most studied materials contain toxic heavy metals such as lead and cadmium.

Acknowledgement

Authors wish to thank S. S. Sarkar (Deputy Director, SEDA), Nilesh Desai (Associate Director, SAC, ISRO), and D. K. Das (Director, SAC, ISRO) for providing the necessary opportunity, facilities and electronic components for carrying out these experiments. Authors also thank Chairman, Department of Physics, Indian Institute of Science, Bangalore and all research scholars of Semiconductor Lab, Department of Physics, IISc for enormous support and motivation.

References

[1] A. Rogalski, Infrared detectors: an overview, Infrared Phys. Technol. 43 (2002) 187–210.
[2] A. Rogalski, J. Antoszewski, L. Faraone, Third generation infrared photodetector arrays, J. Appl. Phys. 105 (2009) 091101.
[3] W. Leia, J. Antoszewski, L. Faraone, Progress, challenges, and opportunities for HgCdTe infrared materials and detectors, Appl. Phys. Rev. 2 (2015) 041303.
[4] AJ. Ciani, RE. Pimpinella, CH. Grein, P.G. Sionnest, Colloidal quantum dots for low–cost MWIR imaging, in: Proc. SPIE 9819, Infrared Technology and Applications XLII, 2016.
[5] A. Chatterjee, N.B. Pendyala, A. Jagtap, K.S.R. Koteswara Rao, Uncooled mid-wave infrared focal plane array using band gap engineered mercury cadmium telluride quantum dot coated silicon ROIC, e-J. Surf. Sci. Nanotechnol. 17 (2019) 95–100.
[6] DJ. Lipomi, JA. Lee, M. Vosgueritchian, BC.-K. Tee, JA. Bolander, Z. Bao, Electronic properties of transparent conductive films of pedot: pss on stretchable substrates, Chem. Mater. 24 (2012) 373–382.
[7] Y. Yang, Y. Zheng, W. Cao, A. Titov, J. Hyvonen, JR. Manders, J. iangengXue, PH. Holloway, L. Qian, High-efficiency light-emitting devices based on quantum dots with tailored nanostructures, Nature Photonics 9 (2015) 259–266.
[8] C-HM. Chuang, PR. Brown, V. Bulović, MG. Bawendi, Improved performance and stability in quantum dot solar cells through band alignment engineering, Nature Mater. 13 (2014) 796–801.
[9] C. Livache, B. Martinez, N. Goubet, C. Gréboval, J. Qu, A. Chu, S. Royer, S. Ithurria, MG. Silly, B. Dubertret, E. Lhuillier, A colloidal quantum dot infrared photodetector and its use for intraband detection, Nature Commun. 10 (2019) 2125.
[10] N. Goubet, C. Livache, B. Martinez, X.Z. Xu, S. Ithurria, S. Royer, H. Cruguel, G. Patriarche, A. Ouerghi, M. Silly, B. Dubertret, E. Lhuillier, Wave-function engineering in HgSe/HgTe colloidal heterostructures to enhance mid-infrared photoconductive properties, Nano Lett. 18 (2018) 4590–4597.
[11] A. Chu, B. Martinez, S. Ferré, V. Noguier, C. Gréboval, C. Livache, J. Qu, Y. Prado, N. Casaretto, N. Goubet, H. Cruguel, L. Dudy, G.S Mathieu, G. Vincent, E. Lhuillier, HgTe nanocrystals for SWIR detection and their integration up to the focal plane array, ACS Appl. Mater. Interfaces 11 (2019) 33116–33123.
[12] A.J. Ciani, R.E. Pimpinella, C.H. Grein, P. Guyot-Sionnest, Colloidal quantum dots for low-cost MWIR imaging, Infrared Technol. Appl. XLII; Int. Soc. Opt. Photon. 9819 (2016) 981919.
[13] A. Chu, B. Martinez, S. Ferré, V. Noguier, C. Gréboval, C. Livache, J. Qu, Y. Prado, N. Casaretto, N.; Goubet, et al., HgTe nanocrystals for SWIR detection and their integration up to the focal plane array, ACS Appl. Mater. Interfaces 11 (2019) 33116–33123.
[14] C. Greboval, S. Ferre, V. Noguier, A. Chu, J. Qu, S.-S. Chee, G. Vincent, E. Lhuillier, Infrared narrow band gap nanocrystals: recent progresses relative to imaging and active detection, arXiv 2001 (2020) 11554 cond-mat, physics: physics.
[15] A. Tittl, A.-K.U. Michel, M. Schäferling, X. Yin, B. Gholipour, L. Cui, M. Wuttig, T. Taubner, F. Neubrech, H. Giessen, A switchable mid-infrared plasmonic perfect absorber with multispectral thermal imaging capability, Adv. Mater. 27 (2015) 4597–4603.
[16] K.-L. Lee, P.-K. Wei, Enhancing surface plasmon detection using ultrasmall nanoslits and a multispectral integration method, Small 6 (2010) 1900–1907.
[17] M. Chen, L. Shao, V. Stephen, HYu Kershaw, W. Jianfang, AL. Rogach, Ni Zhao, Photocurrent enhancement of HgTe quantum dot photodiodes by plasmonic gold nanorod structures, ACS Nano 8 (2014) 8208–8216.
[18] X. Tang, M.M. Ackerman, G. Shen, P. Guyot Sionnest, Towards infrared electronic eyes: flexible colloidal quantum dot photovoltaic detectors enhanced by resonant cavity, Small 15 (2019) 1804920.
[19] B. Zhu, M. Chen, Q. Zhu, G. Zhou, NM. Abdelazim, W. Zhou, SV. Kershaw, AL. Rogach, Ni Zhao, HKi Tsang, Integrated plasmonic infrared photodetector based on colloidal HgTe quantum dots, Adv. Mater. Technol. 4 (2019) 1900354.
[20] MM. Ackerman, X. Tang, P. Guyot-Sionnest, Fast and sensitive colloidal quantum dot mid-wave infrared photodetectors, ACS Nano 12 (2018) 7264–7271.
[21] M. Henini, Molecular beam epitaxy: from research to mass production, Elsevier, Newnes, 31-Dec-2012 - Technology & Engineering.
[22] K. Son, J. Yuan, T. Shen, J. Du, R. Guo, T. Pullerits, J. Tian, Spray coated colloidal quantum dot films for broadband photodetectors, Nanomaterials 9 (2019) 1738.
[23] ME. Cryer, JE. Halpert, 300 nm spectral resolution in the mid-infrared with robust, high responsivity flexible colloidal quantum dot devices at room temperature, ACS Photonics 5 (2018) 3009–3015.
[24] K.S.R. Koteswara RAO, A.P. Abhale, K.P.J. Reddy, Shock Wave Dispersed - Nano Beam Epitaxy (SD-NBE), Indian Patent No. No.6743/CHE/2015 A
[25] J.F. Douglas, J.M. Gasiorek, J.A. Swaffield, L.B. Jack, in: Fluid Mechanics, Pearson, 2005, p. 324. Page.
[26] D. Gaspar, A.C. Pimentel, T. Mateus, J.P. Leita, J. Soares, B.P. Falca, A. Araujo, A. Vicente, S.A. Filonovich, H. Aguas, R. Martins and I. Ferreira, Influence of the layer

thickness in plasmonic gold nanoparticles produced by thermal evaporation, Sci. Reports 3(2013), 1469.
[27] R.A. Maniyara, D. Rodrigo, R. Yu, J. Canet-Ferrer, D.S. Ghosh, R. Yongsunthon, DE. Baker, A. Rezikyan, F. Javier García de Abajo, V. Pruneri, Tunable plasmons in ultrathin metal films, Nature Photonics 13 (2019) 328–333.
[28] ISC9705 Standard 320 Specifications, 400-9705-09 Version 1.3, FLIR Systems Inc.
[29] R.H. Gilmore, E.M.Y. Lee, M.C. Weidman, A.P. Willard, and W. A.Tisdale, Charge carrier hopping dynamics in homogeneously broadened PbS quantum dot solids, Nano Lett. 17(2017), 893.
[30] C. Livache, N. Goubet, B. Martinez, A. Jagtap, J. Qu, S. Ithurria, G.S Mathieu, B. Dubertret, E. Lhuillier, , Band edge dynamics and multiexciton generation in narrow band gap HgTe nanocrystals, ACS Appl. Mater. Interfaces 10 (2018) 11880–11887.
[31] J. Balakrishnan, S. D, M. Siddesh B, A.M. Jagtap, A.P. Abhale, K.S.R. Koteswara Rao, Ternary alloyed HgCdTe nanocrystals for short-wave and mid-wave infrared region optoelectronic applications, Nano Express 1 (2020) 020015.
[32] P.G. Sionnest, M.M. Ackerman, X. Tang, Colloidal quantum dots for infrared detection beyond silicon, J. Chem. Phys. 151 (2019) 060901.

Update

Applied Surface Science Advances

Volume 5, Issue , 1 September 2021, Page

DOI: https://doi.org/10.1016/j.apsadv.2021.100108

Applied Surface Science Advances 5 (2021) 100108

Contents lists available at ScienceDirect

Applied Surface Science Advances

journal homepage: www.elsevier.com/locate/apsadv

Erratum regarding missing Declaration of Competing Interest statements in previously published articles

Declaration of Competing Interest statements were not included in the published version of the following articles that appeared in previous issues of Applied Surface Science Advances.

The appropriate Declaration/Competing Interest statements, provided by the Authors, are included below.

1. "Room temperature operated HgCdTe colloidal quantum dot infrared focal plane array using shockwave dispersion technique" [Applied Surface Science Advances, 2020; 1: 100024] https://doi.org/10.1016/j.apsadv.2020.100024.

   Declaration of competing interest: The Authors have no interests to declare.

2. "Fabrication and characterization of extrinsic electrochemically modified graphite reinforcement carbon paste electrode for selective determination of Cu(II) in trace levels" [Applied Surface Science Advances, 2020; 1: 100031] https://doi.org/10.1016/j.apsadv.2020.100031.

   Declaration of competing interest: The Authors have no interests to declare.

3. "Y–Er–ZrO_2 thermal barrier coatings by EB-PVD: Thermal conductivity, thermal shock life and failure mechanism" [Applied Surface Science Advances, 2021; 3: 100043] https://doi.org/10.1016/j.apsadv.2020.100043.

   Declaration of competing interest: The Authors have no interests to declare.

4. "Integrated solar cells with non-toxic inorganic nanocrystals and polymer bulk heterojunction" [Applied Surface Science Advances, 2021; 3: 100052] https://doi.org/10.1016/j.apsadv.2020.100052.

   Declaration of competing interest: The Authors have no interests to declare.

5. "Morphological and compositional mapping of supersaturated AuNi alloy nanoparticles fabricated by solid state dewetting" [Applied Surface Science Advances, 2021; 4: 100082] https://doi.org/10.1016/j.apsadv.2021.100082.

   Declaration of competing interest: The Authors have no interests to declare.

DOIs of original articles: 10.1016/j.apsadv.2020.100024, 10.1016/j.apsadv.2020.100043, 10.1016/j.apsadv.2021.100082, 10.1016/j.apsadv.2020.100031, 10.1016/j.apsadv.2020.100052

https://doi.org/10.1016/j.apsadv.2021.100108

2666-5239